Inorg. Chem. **2006**, *45*, 4205–4213

Template- and pH-Directed Assembly of Diruthenium Diphosphonates with Different Topologies and Oxidation States

Bin Liu,[†] Ping Yin,[†] Xiao-Yi Yi,[†] Song Gao,[‡] and Li-Min Zheng*[,†]

State Key Laboratory of Coordination Chemistry, Coordination Chemistry Institute, School of Chemistry and Chemical Engineering, Nanjing University, Nanjing 210093, PRC, and State Key Laboratory of Rare Earth Materials and Applications, College of Chemistry and Molecular Engineering, Peking University, Beijing 100871, PRC

Received January 9, 2006

In the presence of organic templates, six diruthenium diphosphonates, namely, $[H_3N(CH_2)_3NH_3]_2[Ru_2(hedp)_2]$ (**1**), $[H_3N(CH_2)_4NH_3]_2[Ru_2(hedp)_2]\cdot 4H_2O$ (**2**), $[H_3N(CH_2)_5NH_3]_2[Ru_2(hedp)_2]\cdot 4H_2O$ (**3**), $[H_3N(CH_2)_3NH_3][Ru_2(hedp)(hedpH)]\cdot H_2O$ (**4**), $[H_3N(CH_2)_4NH_3][Ru_2(hedpH_{0.5})_2]\cdot 2H_2O$ (**5**), and $[H_3N(CH_2)_5NH_3]_2\{[Ru_2(hedp)_2][Ru_2(hedpH)_2]\}$ (**6**) [hedp = 1-hydroxyethylidenediphosphonate, $CH_3C(OH)(PO_3)_2$] have been synthesized under hydrothermal conditions. Compounds **1**–**3** contain homovalent paddlewheel cores of $Ru_2^{II,II}(hedp)_2^{4-}$ that are connected through edge-sharing of the $\{RuO_5Ru\}$ octahedra, resulting in infinite linear chains. Compounds **4**–**6** contain mixed-valent diruthenium(II,III) phosphonate paddlewheel cores of $Ru_2^{II,III}(hedpH_n)_2^{(3-2n)-}$ that are connected by phosphonate oxygen atoms, forming distorted square-grid layers in **4** and **6** or a kagomé lattice in **5**. Both the templates and the pH values are found to play important roles in directing the final products with particular topologies and oxidation states of the diruthenium unit. The magnetic studies show that weak antiferromagentic interactions are propagated between the homovalent diruthenium units in compounds **1**–**3**. For compounds **4**–**6**, weak ferromagnetic interactions are observed.

Introduction

In recent years, a growing interest has been centered on the paramagnetic "paddlewheel" molecules of $Ru_2(O_2CR)_4^{n+}$ in the fields of supramolecular chemistry and molecule-based magnets.[1,2] The mixed-valent diruthenium tetracarboxylate $[Ru_2^{II,III}(O_2CR)_4]^+$ contains three unpaired electrons in an electron configuration of $\sigma^2\pi^4\delta^2\pi^{*2}\delta^{*1}$ with a ground state $S = {}^3/_2$.[3] The ground-state electronic configuration of the homovalent $Ru_2^{II,II}(O_2CR)_4$ is $(\pi^*)^2(\delta^*)^2$ which is an $S = 1$ state.[4] So far, most work has been focused on the more stable mixed-valent $[Ru_2^{II,III}(O_2CR)_4]^+$ species on the basis of which many compounds showing discrete molecular or one-dimensional chain structures have been reported.[1,5−10] The $[Ru_2^{II,III}(O_2CR)_4]^+$ units can also be linked by $M(CN)_6^{3-}$ species, forming compounds $[Ru_2(O_2CCMe_3)_4]_3[M^{III}(CN)_6]\cdot$

* To whom correspondence should be addressed. E-mail: lmzheng@nju.edu.cn. Fax: +86-25-83314502.

[†] Nanjing University.

[‡] Peking University.

(1) (a) Cotton, F. A.; Walton, R. A. *Multiple Bonds between Metal Atoms*, 2nd ed.; Oxford University Press: Oxford, 1993. (b) Aquino, M. A. S. *Coord. Chem. Rev.* **1998**, *170*, 141. (c) Aquino, M. A. S. *Coord. Chem. Rev.* **2004**, *248*, 1025.

(2) Barral, M. C.; Herrero, S.; Jiménez-Aparicio, R.; Torres, M. R.; Urbanos, F. A. *Angew. Chem., Int. Ed.* **2005**, *44*, 305.

(3) Norman, G. J.; Renzoni, G. E.; Case, D. A. *J. Am. Chem. Soc.* **1979**, *101*, 5256.

(4) Cotton, F. A.; Miskowski, V. M.; Zhong, B. *J. Am. Chem. Soc.* **1989**, *111*, 6177.

(5) (a) Bennett, M. J.; Caulton, K. G.; Cotton, F. A. *Inorg. Chem.* **1969**, *8*, 1. (b) Cotton, F. A.; Kim, Y.; Ren, T. *Polyhedron* **1993**, *12*, 607. (c) Barral, M. C.; Jiménez-Aparicio, R.; Pérez-Quintanilla, D.; Pinilla, E.; Priego, J. L.; Royer, E. C.; Urbanos, F. A. *Polyhedron* **1998**, *18*, 371. (d) Cotton, F. A.; Matusz, M.; Zhong, B. *Inorg. Chem.* **1988**, *27*, 4368. (e) Cotton, F. A.; Kim, Y.; Ren, T. *Inorg. Chem.* **1992**, *3*, 2723.

(6) Cukiernik, F. D.; Giroud-Godquin, A. M.; Maldivi, P.; Marchon, J. C. *Inorg. Chim. Acta* **1994**, *215*, 203.

(7) (a) Handa, M.; Sayama, Y.; Mikuriya, M.; Nukada, R.; Hiromitsu, I.; Kasuga, K. *Bull. Chem. Soc. Jpn.* **1995**, *68*, 1647. (b) Handa, M.; Sayama, Y.; Mikuriya, M.; Nukada, R.; Hiromitsu, I.; Kasuga, K. *Chem. Lett.* **1996**, 201. (c) Sayama, Y.; Handa, M.; Mikuriya, M.; Nukada, R.; Hiromitsu, I.; Kasuga, K. *Chem. Lett.* **1998**, 777. (d) Handa, M.; Sayama, Y.; Mikuriya, M.; Nukada, R.; Hiromitsu, I.; Kasuga, K. *Bull. Chem. Soc. Jpn.* **1998**, *71*, 119.

(8) Beck, E. J.; Drysdale, K. D.; Thompson, L. K.; Li, L.; Murphy, C. A.; Aquino, M. A. S. *Inorg. Chim. Acta* **1998**, *279*, 121.

(9) (a) Arribas, G.; Barral, M. C.; González-Prieto, R.; Jiménez-Aparicio, R.; Priego, J. L.; Torres, M. R.; Urbanos, F. A. *Inorg. Chem.* **2005**, *44*, 5770. (b) Barral, M. C.; González-Prieto, R.; Jiménez-Aparicio, R.; Priego, J. L.; Torres, M. R.; Urbanos, F. A. *Eur. J. Inorg. Chem.* **2003**, 2339.

(10) Miyasaka, H.; Clérac, R.; Campos-Fernández, C. S.; Dunbar, K. R. *Inorg. Chem.* **2001**, *40*, 1663.

10.1021/ic060041h CCC: $33.50
Published on Web 04/22/2006

Scheme 1

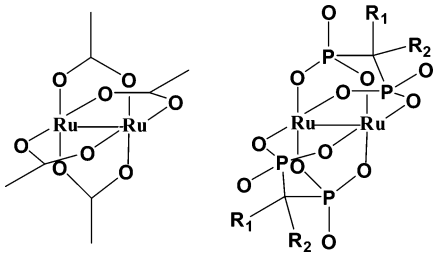

$4H_2O$ (M = Fe, Co, Cr)[11] with two-dimensional layer structures and $[Ru_2(O_2CMe)_4]_3[M^{III}(CN)_6]$ (M = Cr, Fe, Co)[12] with three-dimensional framework structures. Some of them show long-range magnetic ordering at low temperature. The homovalent complexes based on $Ru_2^{II,II}(O_2CR)_4$ are more difficult to obtain mainly because of their air-sensitive nature. The majority of them exist as diadducts in the form of $Ru_2(O_2CR)_4\mathbf{L}_2$, where **L** = THF,[13a−f] 2,2,6,6-tetramethylpiperidine-*N*-oxyl (Temp),[14] Cl,[15] Me_2CO,[13e] H_2O,[4,13e] CH_3CN,[13b] NO,[13f] MeOH,[16] EtOH and H_2O[17] and benzoic acid.[18] There are only three examples, as far as we are aware, that show extended structures including chain compound $[Ru_2(O_2CCF_3)_4(phz)]_\infty$ (phz = phenazine)[19a] and layer compounds $[\{Ru_2(O_2CCF_3)_4\}_2(\mu_4\text{-TCNQ})\cdot 3(C_7H_8)]_\infty$ (TCNQ = 7,7,8,8-tetracyanoquinodimethane)[19b] and $[\{Ru_2(O_2CPh)_4\}_3(trz)_2]_n$ (trz = triazine).[20]

Among the other oxyanions, the phosphonate ligands are promising candidates to be involved in the paddlewheel diruthenium core. By searching the literature, we found that a dinuclear compound $[Ru_2(\mu\text{-}O_2CCH_3)_4(PhPO_3H)_2]H\cdot H_2O$[21] is the only one reported by the other groups in which the phenylphosphonate ligands occupy the axial positions of the diruthenium unit by using one of its three phosphonate oxygen atoms. As shown in Scheme 1, the methylenediphosphonate and its derivatives could have the potential to fully or partially replace the carboxylate ligands in the $Ru_2(O_2CR)_4^{n+}$ core, forming new diruthenium building blocks for the supramolecular assembly. Indeed, compound $(NH_4)_3Ru_2(hedp)_2\cdot 2H_2O$ [hedp = $CH_3C(OH)(PO_3)_2$, 1-hydroxyethylidenediphosphonate] which contains a mixed-valent $Ru_2(hedp)_2^{3-}$ core was prepared successfully.[22a] This compound has a square-grid layer structure, and can be dissolved in aqueous solutions of sodium halide with the stable $Ru_2(hedp)_2^{3-}$ units maintained in solution. Accordingly, linear chain compounds of $Na_4[Ru_2(hedp)_2X]\cdot 16H_2O$ [X = Cl, Br] and $Na_7[Ru_2(hedp)_2Fe(CN)_6]\cdot 24H_2O$ were isolated from aqueous solution.[22b] In this paper, we report that the topologies of the $Ru_2(hedp)_2^{3-}$-based compounds may be manipulated by the introduction of different organic diamines, and homovalent species of $Ru_2^{II,II}(hedp)_2^{4-}$ may be stabilized simply by adjusting the pH of the reaction mixtures. Six compounds are described, namely, $[H_3N(CH_2)_3NH_3]_2[Ru_2(hedp)_2]$ (**1**), $[H_3N(CH_2)_4NH_3]_2[Ru_2(hedp)_2]\cdot 4H_2O$ (**2**), $[H_3N(CH_2)_5NH_3]_2[Ru_2(hedp)_2]\cdot 4H_2O$ (**3**), $[H_3N(CH_2)_3NH_3][Ru_2(hedp)(hedpH)]\cdot H_2O$ (**4**), $[H_3N(CH_2)_4NH_3][Ru_2(hedpH_{0.5})_2]\cdot 2H_2O$ (**5**), and $[H_3N(CH_2)_5NH_3]_2[Ru_2(hedp)_2][Ru_2(hedpH)_2]$ (**6**). To our knowledge, compounds **1**−**3** are the first examples of diruthenium diphosphonates with homovalent $Ru_2^{II,II}$ oxidation states, whereas in compounds **4**−**6**, mixed-valent $Ru_2^{II,III}$ cores are observed. The structure and magnetic properties of compound **5** with a kagomé lattice have already been reported in a Communication.[22c]

Experimental Section

Materials and Methods. All the starting materials were of reagent grade and were obtained from commercial sources without further purification. Elemental analyses were performed in a PE240C elemental analyzer. The infrared spectra were recorded on a VECTOR 22 spectrometer with pressed KBr pellets. Thermal analyses were performed in nitrogen with a heating rate of 20 °C/min on a TGA-DTA V1.1 TA Inst 2100 instrument. The powder XRD patterns were recorded on a Shimadzu XD-3A X-ray diffractometer. Variable-temperature magnetic susceptibility data were obtained on polycrystalline samples (44.95 mg for **1**, 28.10 mg for **2**, 7.02 mg for **3**, 15.08 mg for **4**, 29.45 mg for **6**) using a Quantum Design MPMS-XL7 SQUID magnetometer. Diamagnetic corrections were obtained from Pascal's constants.[23]

Synthesis of $[H_3N(CH_2)_3NH_3]_2[Ru_2(hedp)_2]$ (1). A mixture of $RuCl_3\cdot 3.5H_2O$ (0.1146 g 0.42 mmol), $hedpH_4\cdot H_2O$ (0.4702 g 2.10 mmol) and H_2O (6 cm^3), adjusted by 1,3-diaminopropane to pH = 6.20, was kept in a Teflon-lined autoclave at 140 °C for 9 days. After the mixture was slowly cooled to room temperature, dark brown columnlike crystals were collected as a monophasic material, as judged by the powder X-ray diffraction pattern. Yield: 0.0350 g (22% based on Ru). Anal. Calcd for $C_{10}H_{32}N_4O_{14}P_4Ru_2$: C, 15.84; H, 4.25; N, 7.39. Found: C, 15.86; H, 4.27; N, 7.33%. IR (KBr, cm^{-1}): 3552(w), 3443(br, s), 3070(s), 2989(s), 2970(s), 2931(br, s), 2726(s), 2587(m), 2513(m), 1644(s), 1597(m), 1540(w),

(11) (a) Yoshioka, D.; Mikuriya, M.; Handa, M. *Chem. Lett.* **2002**, 1044. (b) Vos, T. E.; Miller, J. S. *Angew. Chem., Int. Ed.* **2005**, *44*, 2.

(12) (a) Liao, Y.; Shum, W. W.; Miller, J. S. *J. Am. Chem. Soc.* **2002**, *124*, 9336. (b) Vos, T. E.; Liao, Y.; Shum, W. W.; Her, J.-H.; Stephens, P. W.; Reiff, W. M.; Miller, J. S. *J. Am. Chem. Soc.* **2004**, *126*, 11630.

(13) (a) Furukawa, S.; Kitagawa, S. *Inorg. Chem.* **2004**, *43*, 6464. (b) Chisholm, M. H.; Christou, G.; Folting, K.; Huffman, J. C.; James, C. A.; Samuels, J. A.; Wesemann, J. L.; Woodruff, W. H. *Inorg. Chem.* **1996**, *35*, 3643. (c) Barral, M. C.; Jiménez-Aparicio, R.; Priego, J. L.; Royer, E. C.; Urbanos, F. A.; Amador, U. *Inorg. Chim. Acta* **1998**, *279*, 30. (d) Lindsay, A. J.; Tooze, R. P.; Motevalli, M.; Hursthouse, M. B.; Wilkinson, G. *J. Chem. Soc. Chem. Commun.* **1984**, 1383. (e) Lindsay, A. J.; Wilkinson, G.; Motevalli, M.; Hursthouse, M. B. *J. Chem. Soc., Dalton. Trans.* **1985**, 2321. (f) Lindsay, A. J.; Wilkinson, G.; Motevalli, M.; Hursthouse, M. B. *J. Chem. Soc., Dalton. Trans.* **1987**, 2723.

(14) Cogne, A.; Belorizky, E.; Laugier, J.; Rey, P. *Inorg. Chem.* **1994**, *33*, 3363.

(15) Das, B. K.; Chakravarty, A. R. *Inorg. Chem.* **1992**, *31*, 1395.

(16) Cotton, F. A.; Labella, L.; Shang, M.-Y. *Inorg. Chim. Acta* **1992**, *197*, 149.

(17) Cotton, F. A.; Daniels, L. M.; Kibala, P. A.; Matusz, M.; Roth, W. J.; Schwotzer, W.; Wang, W.-N.; Zhong, B. *Inorg. Chim. Acta* **1994**, *215*, 9.

(18) Spohn, M.; Strähle, J.; Hiller, W. *Z. Naturforsch., B: Chem. Sci.* **1986**, *41*, 541.

(19) (a) Miyasaka, H.; Clérac, R.; Campos-Fernández, C. S.; Dunbar, K. R. *J. Chem. Soc., Dalton Trans.* **2001**, 858. (b) Miyasaka, H.; Campos-Fernández, C. S.; Clérac, R.; Dunbar, K. R. *Angew. Chem., Int. Ed.* **2000**, *39*, 3831.

(20) Furukawa, S.; Ohba, M.; Kitagawa, S. *Chem. Commun.* **2005**, 865.

(21) McCann, M.; Murphy, E.; Cardin, C.; Convery, M. *Polyhedron* **1993**, *12*, 1725.

(22) (a) Yi, X.-Y.; Zheng, L.-M.; Xu, W.; Feng, S.-H. *Inorg. Chem.* **2003**, *42*, 2827. (b) Yi, X.-Y.; Liu, B.; Jiménez-Aparicio, R.; Urbanos, F. A.; Gao, S.; Xu, W.; Chen, J.-S.; Song, Y.; Zheng, L.-M. *Inorg. Chem.* **2005**, *44*, 4309. (c) Liu, B.; Li, Y.-Z.; Zheng, L.-M. *Inorg. Chem.* **2005**, *44*, 6921.

(23) Kahn, O. *Molecular Magnetism*; VCH Publishers: New York, 1993.

1513(s), 1474(m), 1412(w), 1391(m), 1362(w), 1333(w), 1237(m), 1210(m), 1146(s), 1127(s), 1099(vs), 1077(vs), 1035(vs), 1009(s), 972(vs), 926(s), 916(s), 848(w), 826(m), 774(m), 756(m), 654(m), 579(vs), 494(s), 468(m), 453(m), 416(w). Thermal analysis shows that the weight loss in the temperature range 20−260 °C is zero, in agreement with the single-crystal structural determination.

Synthesis of $[H_3N(CH_2)_4NH_3]_2[Ru_2(hedp)_2]\cdot 4H_2O$ (2). A mixture of $RuCl_3\cdot 3.5H_2O$ (0.0352 g 0.13 mmol), $hedpH_4\cdot H_2O$ (0.1469 g 0.66 mmol) and H_2O (2 cm^3), adjusted by 1,4-diaminobutane to pH = 6.10, was kept in a Teflon-lined autoclave at 140 °C for 8 days. After the mixture was slowly cooled to room temperature, dark brown columnlike crystals were collected as a monophasic material, as judged by the powder X-ray diffraction pattern. Yield: 0.0163 g (33% based on Ru). Anal. Calcd for $C_{12}H_{44}N_4O_{18}P_4Ru_2$: C, 16.78; H, 5.16; N, 6.53. Found: C, 16.31; H, 5.22; N, 6.85%. IR (KBr, cm^{-1}): 3522(w), 3448(br, s), 3070(s), 2989(s), 2970(s), 2931(br, s), 2727(m), 2587(m), 2514(m), 1644(s), 1597(m), 1541(w), 1513(s), 1475(m), 1412(w), 1390(m), 1364(w), 1333(w), 1237(m), 1210(m), 1145(s), 1127(s), 1099(vs), 1077(vs), 1036(vs), 10011(s), 972(vs), 927(s), 917(s), 849(w), 827(m), 775(m), 757(m), 654(m), 579(vs), 494(s), 468(m), 453(m), 416(w). Thermal analysis shows that the weight loss in the temperature range 20−165 °C is 8.7%, in agreement with the calculated value for the release of four water molecules (8.4%).

Synthesis of $[H_3N(CH_2)_5NH_3]_2[Ru_2(hedp)_2]\cdot 4H_2O$ (3). A mixture of $RuCl_3$ (0.0707 g 0.34 mmol), $hedpH_4\cdot H_2O$ (0.3808 g 1.70 mmol) and H_2O (4 cm^3), adjusted by 1,5-diaminopentane to pH = 6.05, was kept in a Teflon-lined autoclave at 140 °C for 10 days. After the mixture was slowly cooled to room temperature, dark brown columnlike crystals were collected as a monophasic material, as judged by the powder X-ray diffraction pattern. Yield: 0.0600 g (41% based on Ru). Anal. Calcd for $C_{14}H_{48}N_4O_{18}P_4Ru_2$: C, 18.97; H, 5.46; N, 6.32. Found: C, 19.26; H, 5.57; N, 6.31%. IR (KBr, cm^{-1}): 3193(br, s), 2957(s), 2923(s), 2864(s), 2546(m), 2067(w), 1634(s), 1595(m), 1528(s), 1459(m), 1445(w), 1355(s), 1310(w), 1269(w), 1238(w), 1144(vs), 1127(vs), 1115(s), 1094(vs), 1076-(vs), 1032(vs), 1003(s), 965(vs), 922(s), 907(m), 867(w), 819(m), 715(m), 649(m), 576(vs), 494(s), 466(m). Thermal analysis shows that the weight loss in the temperature range 20−140°C is 8.4%, in agreement with the calculated value for the release of four water molecules (8.1%).

Synthesis of $[H_3N(CH_2)_3NH_3][Ru_2(hedp)(hedpH)]\cdot H_2O$ (4). A mixture of $RuCl_3\cdot 3.5H_2O$ (0.0405 g 0.15 mmol), $hedpH_4\cdot H_2O$ (0.1686 g 0.75 mmol) and H_2O (2 cm^3), adjusted by 1,3-diaminopropane to pH = 2.78, was kept in a Teflon-lined autoclave at 140 °C for 6 days. After the mixture was slowly cooled to room temperature, square platelike brown-red crystals were collected as a monophasic material, as judged by the powder X-ray diffraction pattern. Yield: 0.0424 g (81% based on Ru). Anal. Calcd for $C_7H_{23}N_2O_{15}P_4Ru_2$: C, 11.99; H, 3.31; N, 3.99. Found: C, 11.33; H, 3.44; N, 4.02%. IR (KBr, cm^{-1}): 3549(m), 3430(br, s), 3169-(br, s), 3030(m), 2982(m), 2931(m), 1648(m), 1613(s), 1583(m), 1545(m), 1520(s), 1458(m), 1408(w), 1364(w), 1324(m), 1108(vs), 1041(s), 907(vs), 902(s), 803(s), 758(w), 649(m), 579(vs), 486(s), 454(m), 439(m). Thermal analysis shows that the weight loss in the temperature range 20−180 °C is 2.6%, in agreement with the calculated value for the release of one water molecule (2.6%).

Synthesis of $[H_3N(CH_2)_5NH_3]_2[Ru_2(hedp)_2][Ru_2(hedpH)_2]$ (6). A mixture of $RuCl_3\cdot 3.5H_2O$ (0.0442 g 0.16 mmol), $hedpH_4\cdot H_2O$ (0.1104 g 0.49 mmol) and H_2O (3 cm^3), adjusted by 1,5-diaminopentane to pH = 4.53, was kept in a Teflon-lined autoclave at 140 °C for 6 days. After the mixture was slowly cooled to room temperature, square platelike brown-red crystals were collected as a monophasic material, as judged by the powder X-ray diffraction pattern. Yield: 0.0307 g (52% based on Ru). Anal. Calcd for $C_9H_{25}N_2O_{14}P_4Ru_2$: C, 15.19; H, 3.54; N, 3.94. Found: C, 14.83; H, 3.61; N, 4.22%. IR (KBr, cm^{-1}): 3405(m), 3197(br, s), 3162(br, s), 2941(m), 1616(m), 1595(s), 1507(s), 1449(m), 1402-(w), 1370(w), 1115(vs), 1104(vs), 971(vs), 938(vs), 909(s), 799-(s), 652(w), 591(s), 583(s), 546(m), 508(m), 480(s), 435(m). Thermal analysis shows no weight loss in the temperature range 20−180 °C, in agreement with the single-crystal structural determination.

Crystallographic Studies. Single crystals of dimensions 0.30 × 0.10 × 0.10 mm^3 for **1**, 0.20 × 0.06 × 0.06 mm^3 for **2**, 0.10 × 0.02 × 0.02 mm^3 for **3**, 0.25 × 0.05 × 0.05 mm^3 for **4**, and 0.20 × 0.15 × 0.15 mm^3 for **6** were used for structural determinations on a Bruker SMART APEX CCD diffractometer using graphite-monochromatized Mo Kα radiation (λ = 0.71 073 Å) at room temperature. A hemisphere of data was collected in the θ range 2.27−28.04° for **1**, 1.88−28.06° for **2**, 1.80−28.03° for **3**, 2.00−27.98° for **4**, and 2.54−28.02° for **6**, using a narrow-frame method with scan widths of 0.30° in ω and an exposure time of 10 s/frame. Numbers of observed and unique reflections are 6987 and 2862 (R_{int} = 0.0805) for **1**, 8343 and 3253 (R_{int} = 0.0652) for **2**, 8779 and 3439 (R_{int} = 0.0807) for **3**, 4958 and 3633 (R_{int} = 0.0716) for **4**, and 7402 and 2829 (R_{int} = 0.0658) for **6**, respectively. The data were integrated using the Siemens SAINT program,[24] with the intensities corrected for Lorentz factor, polarization, air absorption, and absorption due to variation in the path length through the detector faceplate. The structures were solved by direct methods and refined on F^2 by full-matrix least-squares using SHELXTL.[25] All the non-hydrogen atoms were refined anisotropically. All the hydrogen atoms, except those of hydroxy groups and water molecules, were placed in calculated positions. The hydrogen atoms of hydroxy groups and water molecules were located from the difference Fourier maps and refined isotropically with the isotropic vibration parameters related to the non-hydrogen atom to which they are bonded. Crystallographic and refinement details of compounds **1**−**6** are listed in Table 1, the selected bond lengths and angles are listed in Tables 2−7.

Results and Discussion

Syntheses. Compounds **1**−**6** were prepared through hydrothermal reactions of $RuCl_3$ and $hedpH_4$ in the presence of organic diamines at 140 °C. As is well-known, a number of factors involved in the hydrothermal reactions can affect the final products, including the reaction temperature, molar ratio of the starting materials, the presence of templates, and pH, etc. In this work, we find that both the templates and the pH of the reaction mixture play crucial roles in the formation of **1**−**6**.

By using 1,3-diaminopropane as a template, compound **4** was obtained as red-brown platelike crystals when the molar ratio of $hedpH_4/RuCl_3$ is 3:1 and the pH is 2.78. A single phase of the same compound can be obtained when the pH is 2.5 to ∼4.0. Similar reactions at a lower pH (<2.5) produce a mixture of **4** and metal Ru impurities. When the pH is higher (4.0 to ∼5.8), a mixture of mixed-valent compound

(24) *SAINT, Program for Data Extraction and Reduction;* Siemens Analytical X-ray Instruments Inc.; Madison, WI, 1994−1996.
(25) Sheldrick, G. M. *SHELXTL, Program for Refinement of Crystal Structures;* Siemens Analytical X-ray Instruments Inc.: Madison, WI, 1994.

Table 1. Crystallographic Data

cmpd	**1**	**2**	**3**	**4**	**5**	**6**
formula	$C_{10}H_{32}N_4O_{14}P_4Ru_2$	$C_{12}H_{44}N_4O_{18}P_4Ru_2$	$C_{14}H_{46}N_4O_{18}P_4Ru_2$	$C_7H_{23}N_2O_{15}P_4Ru_2$	$C_8H_{27}N_2O_{16}P_4Ru_2$	$C_9H_{25}N_2O_{14}P_4Ru_2$
mol wt	758.42	858.53	884.57	701.29	733.34	711.33
cryst syst	monoclinic	monoclinic	monoclinic	orthorhombic	trigonal	triclinic
space group	*C*2/*c*	$P2_1/n$	$P2_1/n$	$Pca2_1$	$P\bar{3}1c$	$P\bar{1}$
a (Å)	22.919(4)	5.5596(7)	5.4585(8)	20.378(4)	14.3827(19)	9.792(2)
b (Å)	5.3529(9)	19.343(3)	19.101(3)	9.7947(18)	14.3827(19)	10.147(2)
c (Å)	18.991(3)	13.0498(17)	14.0445(19)	10.0517(19)	19.992(4)	12.077(3)
α (deg)						66.126(4)
β (deg)	108.937(3)	91.347(3)	91.598(3)			67.096(4)
γ (deg)						88.068(4)
V (Å^3)	2203.8(6)	1403.0(3)	1463.7(4)	2006.3(6)	3581.5(9)	999.8(4)
Z	4	2	2	4	6	2
D_c (g cm^{-3})	2.286	2.032	2.007	2.322	2.040	2.363
F(000)	1520	872	900	1388	2190	706
μ(Mo Kα) (cm^{-1})	17.40	13.90	13.35	19.02	16.06	19.07
GOF on F^2	1.111	0.749	0.887	1.125	1.045	1.076
R1, wR2[a] [$I > 2\sigma(I)$]	0.0612, 0.1064	0.0424, 0.0582	0.0598, 0.0783	0.0421, 0.0849	0.0450, 0.0752	0.0624, 0.1302
R1, wR2 (all data)	0.0852, 0.1137	0.0734, 0.0632	0.1114, 0.0892	0.0482, 0.0866	0.0696, 0.0790	0.0894, 0.1352
$\Delta\rho_{max}$, $\Delta\rho_{min}$ (e Å^{-3})	1.056, −1.246	0.816, −0.690	0.932, −1.531	0.626, −0.676	0.826, −0.831	0.741, −1.615

[a] R1 $=\sum||F_o| - |F_c||/\sum|F_o|$, wR2 $= [\sum w(F_o^2 - F_c^2)^2/\sum w(F_o^2)^2]^{1/2}$.

Table 2. Selected Bond Lengths [Å] and Angles [deg] for **1**[a]

Ru(1)−O(4)	2.065(4)	Ru(1)−O(5A)	2.074(4)
Ru(1)−O(1)	2.063(4)	Ru(1)−O(5B)	2.373(4)
Ru(1)−O(2A)	2.091(4)	Ru(1)−Ru(1A)	2.3297(11)
P(2)−O(4)	1.539(4)	P(2)−O(6)	1.497(4)
P(2)−O(5)	1.546(4)	P(1)−O(1)	1.543(5)
P(1)−O(2)	1.541(5)	P(1)−O(3)	1.516(4)
O(1)−Ru(1)−O(4)	91.85(17)	O(1)−Ru(1)−O(5A)	88.81(16)
O(4)−Ru(1)−O(5A)	174.63(16)	O(1)−Ru(1)−O(2A)	174.70(17)
O(4)−Ru(1)−O(2A)	88.51(16)	O(5A)−Ru(1)−O(2A)	90.35(16)
O(1)−Ru(1)−Ru(1A)	92.13(12)	O(4)−Ru(1)−Ru(1A)	92.03(12)
O(5A)−Ru(1)−Ru(1A)	93.27(12)	O(2A)−Ru(1)−Ru(1A)	93.14(12)
O(1)−Ru(1)−O(5B)	87.06(16)	O(4)−Ru(1)−O(5B)	95.08(15)
O(5A)−Ru(1)−O(5B)	79.63(16)	O(2A)−Ru(1)−O(5B)	87.65(15)
Ru(1A)−Ru(1)−O(5B)	172.87(10)	Ru(1A)−O(5)−Ru(1C)	100.37(16)
P(2)−O(4)−Ru(1)	113.8(2)	P(2)−O(5)−Ru(1A)	112.6(2)
P(2)−O(5)−Ru(1C)	140.3(2)	P(1)−O(1)−Ru(1)	113.2(2)
P(1)−O(2)−Ru(1A)	111.4(2)		

[a] Symmetry codes: (A) $-x + 1/2, -y + 1/2, -z$; (B) $x, y - 1, z$; (C) $x, y + 1, z$.

Table 3. Selected Bond Lengths [Å] and Angles [deg] for **2**[a]

Ru(1)−O(1)	2.090(3)	Ru(1)−O(2A)	2.076(3)
Ru(1)−O(4)	2.063(3)	Ru(1)−O(5A)	2.105(3)
Ru(1)−Ru(1A)	2.3380(8)	Ru(1)−O(5B)	2.514(3)
P(1)−O(1)	1.547(3)	P(2)−O(4)	1.539(3)
P(1)−O(2)	1.530(3)	P(2)−O(5)	1.547(3)
P(1)−O(3)	1.503(3)	P(2)−O(6)	1.494(3)
O(4)−Ru(1)−O(1)	91.59(11)	O(4)−Ru(1)−O(2A)	88.92(10)
O(1)−Ru(1)−O(2A)	174.73(11)	O(4)−Ru(1)−O(5A)	174.94(11)
O(1)−Ru(1)−O(5A)	89.28(10)	O(2A)−Ru(1)−O(5A)	89.76(10)
O(4)−Ru(1)−Ru(1A)	89.77(8)	O(1)−Ru(1)−Ru(1A)	91.52(8)
O(2A)−Ru(1)−Ru(1A)	93.73(8)	O(5A)−Ru(1)−Ru(1A)	95.19(8)
O(1)−Ru(1)−O(5B)	87.57(10)	O(4)−Ru(1)−O(5B)	96.61(10)
O(2A)−Ru(1)−O(5B)	87.16(10)	O(5B)−Ru(1)−O(5A)	78.45(10)
Ru(1A)−Ru(1)−O(5B)	173.58(6)	Ru(1A)−O(5B)−Ru(1C)	101.55(10)
P(1)−O(1)−Ru(1)	112.51(16)	P(1)−O(2)−Ru(1A)	111.70(15)
P(2)−O(5)−Ru(1A)	110.50(16)	P(2)−O(4)−Ru(1)	116.60(15)
P(2)−O(5)−Ru(1A)	110.50(15)		

[a] Symmetry codes: (A) $-x + 1, -y + 1, -z + 1$; (B) $x + 1, y, z$; (C) $x - 1, y, z$.

4 and homovalent compound **1** results. Further increase of pH (∼6.2) promotes the formation of dark brown columnlike crystals of compound **1** as a pure phase when the molar ratio of $hedpH_4/RuCl_3$ is 5:1. When the pH is greater than 6.20, only a clear solution is obtained.

Table 4. Selected Bond Lengths [Å] and Angles [deg] for **3**[a]

Ru(1)−O(1)	2.086(4)	Ru(1)−O(2A)	2.073(4)
Ru(1)−O(4)	2.071(4)	Ru(1)−O(5B)	2.446(5)
Ru(1)−O(5A)	2.092(4)	Ru(1)−Ru(1A)	2.3295(11)
P(1)−O(1)	1.547(3)	P(1)−O(2)	1.530(3)
P(1)−O(3)	1.503(3)	P(2)−O(4)	1.539(3)
P(2)−O(5)	1.547(3)	P(2)−O(6)	1.494(3)
O(4)−Ru(1)−O(1)	90.84(16)	O(4)−Ru(1)−O(2A)	89.88(16)
O(1)−Ru(1)−O(2A)	174.44(18)	O(4)−Ru(1)−O(5A)	174.72(18)
O(1)−Ru(1)−O(5A)	89.60(16)	O(2A)−Ru(1)−O(5A)	89.17(15)
O(4)−Ru(1)−Ru(1A)	90.30(12)	O(1)−Ru(1)−Ru(1A)	92.53(12)
O(2A)−Ru(1)−Ru(1A)	92.98(12)	O(5A)−Ru(1)−Ru(1A)	94.93(12)
O(4)−Ru(1)−O(5B)	95.04(15)	O(1)−Ru(1)−O(5B)	88.50(15)
O(2A)−Ru(1)−O(5B)	85.94(15)	O(5A)−Ru(1)−O(5B)	79.71(16)
Ru(1A)−Ru(1)−O(5B)	174.54(10)	Ru(1A)−O(5)−Ru(1C)	100.29(16)
P(1)−O(1)−Ru(1)	112.0(2)	P(1)−O(2)−Ru(1A)	112.7(2)
P(1)−O(2)−Ru(1C)	140.8(2)	P(2)−O(4)−Ru(1)	116.3(2)
P(2)−O(5)−Ru(1A)	111.1(2)		

[a] Symmetry codes: (A) $-x + 1, -y + 1, -z + 1$; (B) $x + 1, y, z$; (C) $x - 1, y, z$.

By using 1,4-diaminobutane as a template, red-brown hexagonal block crystals of mixed-valent compound **5** and dark brown columnlike crystals of homovalent compound **2** can be prepared similarly as single phases when the pH is 2.57 and 6.10, respectively. When the pH is less than 2.5, a mixture of compound **5** and Ru impurities is produced. Reactions at pH greater than 6.5 result in a clear solution. Single phases of the mixed-valent compound **6** and homovalent compound **3** can be synthesized in the presence of 1,5-diaminopentane when the pH equals 4 to ∼5 and 6.05, respectively. When the pH is 2.5 to ∼4, compound **6** appears as a red-brown powder together with an unrecognized impurity, as judged by IR and powder XRD. A lower pH (<2.5) favors Ru impurities besides **6**. Compound **3** becomes dominant at a pH greater than 5.5. When the pH is greater than 6.30, a clear solution is again observed.

Description of Structure 1. Compound **1** crystallizes in monoclinic space group *C*2/*c*. The structure consists of

Table 5. Selected Bond Lengths [Å] and Angles [deg] for **4**[a]

Ru(1)−O(1)	2.019(6)	Ru(1)−O(4)	2.027(6)
Ru(1)−O(8)	2.030(5)	Ru(1)−O(11)	2.019(6)
Ru(1)−O(3A)	2.245(6)	Ru(1)−Ru(2)	2.360(1)
Ru(2)−O(2)	2.040(5)	Ru(2)−O(5)	2.050(6)
Ru(2)−O(12)	2.052(6)	Ru(2)−O(9)	2.055(5)
Ru(2)−O(13B)	2.245(6)	P(1)−O(1)	1.522(6)
P(1)−O(2)	1.546(6)	P(1)−O(3)	1.480(6)
P(2)−O(4)	1.534(6)	P(2)−O(5)	1.544(6)
P(2)−O(6)	1.491(5)	P(3)−O(8)	1.530(5)
P(3)−O(9)	1.526(7)	P(3)−O(10)	1.544(5)
P(4)−O(11)	1.523(6)	P(4)−O(12)	1.545(6)
P(4)−O(13)	1.501(6)		
O(1)−Ru(1)−O(11)	176.1(3)	O(1)−Ru(1)−O(4)	88.0(2)
O(11)−Ru(1)−O(4)	91.6(2)	O(1)−Ru(1)−O(8)	91.8(2)
O(11)−Ru(1)−O(8)	88.3(2)	O(4)−Ru(1)−O(8)	175.3(2)
O(1)−Ru(1)−O(3A)	91.7(2)	O(11)−Ru(1)−O(3A)	84.5(2)
O(4)−Ru(1)−O(3A)	90.0(2)	O(8)−Ru(1)−O(3A)	85.2(2)
O(1)−Ru(1)−Ru(2)	91.4(2)	O(11)−Ru(1)−Ru(2)	92.5(2)
O(4)−Ru(1)−Ru(2)	92.1(2)	O(8)−Ru(1)−Ru(2)	92.7(1)
O(3A)−Ru(1)−Ru(2)	176.4(1)	O(2)−Ru(2)−O(5)	91.4(2)
O(2)−Ru(2)−O(12)	174.7(2)	O(5)−Ru(2)−O(12)	87.2(2)
O(2)−Ru(2)−O(9)	88.9(2)	O(5)−Ru(2)−O(9)	175.0(2)
O(12)−Ru(2)−O(9)	92.0(2)	O(2)−Ru(2)−O(13B)	85.7(2)
O(5)−Ru(2)−O(13B)	89.1(2)	O(12)−Ru(2)−O(13B)	89.1(2)
O(9)−Ru(2)−O(13B)	85.9(2)	O(2)−Ru(2)−Ru(1)	93.3(2)
O(5)−Ru(2)−Ru(1)	92.5(2)	O(12)−Ru(2)−Ru(1)	91.8(2)
O(9)−Ru(2)−Ru(1)	92.4(2)	O(13B)−Ru(2)−Ru(1)	178.1(2)
P(1)−O(1)−Ru(1)	115.8(3)	P(1)−O(2)−Ru(2)	112.2(3)
P(1)−O(3)−Ru(1C)	138.7(4)	P(2)−O(4)−Ru(1)	114.3(3)
P(2)−O(5)−Ru(2)	111.9(3)	P(3)−O(8)−Ru(1)	112.3(3)
P(3)−O(9)−Ru(2)	111.1(3)	P(4)−O(11)−Ru(1)	114.7(3)
P(4)−O(12)−Ru(2)	112.6(3)	P(4)−O(13)−Ru(2D)	138.6(3)

[a] Symmetry codes: (A) $-x+3/2, y, z-1/2$; (B) $-x+1, -y+1, z+1/2$; (C) $-x+3/2, y, z+1/2$; (D) $-x+1, -y+1, z-1/2$.

Table 6. Selected Bond Lengths [Å] and Angles [deg] for **5**[a]

Ru(1)−O(1)	2.050(3)	Ru(1)−O(2A)	2.020(3)
Ru(1)−O(5A)	2.018(3)	Ru(1)−O(4)	2.066(3)
Ru(1)−O(3B)	2.237(3)	Ru(1)−Ru(1A)	2.351(1)
P(1)−O(1)	1.536(3)	P(1)−O(2)	1.543(3)
P(1)−O(3)	1.503(3)	P(2)−O(4)	1.529(3)
P(2)−O(5)	1.555(3)	P(2)−O(6)	1.510(3)
O(5A)−Ru(1)−O(2A)	91.2(1)	O(5A)−Ru(1)−O(1)	88.7(1)
O(2A)−Ru(1)−O(1)	175.3(1)	O(5A)−Ru(1)−O(4)	175.1(1)
O(2A)−Ru(1)−O(4)	88.9(1)	O(1)−Ru(1)−O(4)	90.8(1)
O(5A)−Ru(1)−O(3B)	84.1(1)	O(2A)−Ru(1)−O(3B)	83.1(1)
O(1)−Ru(1)−O(3B)	92.2(1)	O(4)−Ru(1)−O(3B)	91.1(1)
O(5A)−Ru(1)−Ru(1A)	93.0(1)	O(2A)−Ru(1)−Ru(1A)	92.0(1)
O(1)−Ru(1)−Ru(1A)	92.8(1)	O(4)−Ru(1)−Ru(1A)	91.9(1)
O(3B)−Ru(1)−Ru(1A)	174.2(1)	P(1)−O(1)−Ru(1)	112.6(2)
P(1)−O(2)−Ru(1A)	114.3(2)	P(1)−O(3)−Ru(1C)	143.5(2)
P(2)−O(4)−Ru(1)	112.4(2)	P(2)−O(5)−Ru(1A)	112.9(2)

[a] Symmetry codes: (A) $-x+1, -y+2, -z+2$; (B) $-y+1, x-y-1, z$; (C) $-x+y, -x+1, z$.

$[NH_3(CH_2)_3NH_3]^{2+}$ cations and homovalent diruthenium(II,II) chains of $\{Ru_2(hedp)_2\}_n^{4n-}$. A detail of the chain is illustrated in (Figure 1). Clearly, the building unit $Ru_2(hedp)_2^{4-}$ has a paddlewheel geometry similar to the mixed-valent $Ru_2(hedp)_2^{3-}$ unit in $(NH_4)_3Ru_2(hedp)_2\cdot 2H_2O$.[22a] The Ru atom has a slightly distorted octahedral environment. Each $\{RuO_5Ru\}$ octahedron shares its five vertexes with five CPO_3 units from three equivalent $hedp^{4-}$ groups. The remaining position is filled with the equivalent Ru(1A) atom. The Ru−O bond lengths fall in the range of 2.063(4)−2.373(4) Å, and the Ru(1)−Ru(1A) distance is 2.330(1) Å. The angles around the Ru atom are between 79.6(2) and 95.1(2)°. The O(5A)−Ru(1)−O(5B) angle [79.6(2)°] is apparently smaller than the other O−Ru−O(Ru) angles because of the formation of a four-member ring (Figure 1). The Ru−Ru distance in **1**, although slightly shorter than that in $(NH_4)_3Ru_2(hedp)_2\cdot 2H_2O$ [Ru(1)−Ru(1A), 2.347(1) Å], is apparently longer than those found in the other homovalent Ru_2^{4+} complexes such as $[Ru_2(O_2CCF_3)_4(phz)]_\infty$ [2.3109 Å] and $[\{Ru_2(O_2CCF_3)_4\}_2(\mu_4\text{-TCNQ})\cdot 3(C_7H_8)]_\infty$ [2.2875 Å].[19] The large bite of the $hedp^{4-}$ ligand [O(1)···O(2) 2.521 Å, O(4)···O(5) 2.521 Å] and the axial interactions should be responsible for the lengthening of Ru−Ru in compound **1** compared with those of diruthenium(II,II) tetracarboxylates.

Table 7. Selected Bond Lengths [Å] and Angles [deg] for **6**[a]

Ru(1)−O(4)	2.025(5)	Ru(1)−O(5A)	2.036(4)
Ru(1)−O(1)	2.028(5)	Ru(1)−O(10B)	2.278(5)
Ru(1)−O(2A)	2.033(5)	Ru(1)−Ru(1A)	2.346(1)
Ru(2)−O(8)	2.033(5)	Ru(2)−O(3)	2.299(5)
Ru(2)−O(9C)	2.031(5)	Ru(2)−O(11)	2.050(5)
Ru(2)−O(12C)	2.027(5)	Ru(2)−Ru(2C)	2.366(1)
P(1)−O(1)	1.521(6)	P(1)−O(2)	1.555(5)
P(1)−O(3)	1.494(5)	P(2)−O(4)	1.535(6)
P(2)−O(5)	1.539(5)	P(2)−O(6)	1.497(5)
P(3)−O(8)	1.535(5)	P(3)−O(9)	1.536(5)
P(3)−O(10)	1.494(5)	P(4)−O(11)	1.534(5)
P(4)−O(12)	1.527(6)	P(4)−O(13)	1.515(5)
O(4)−Ru(1)−O(1)	90.5(2)	O(4)−Ru(1)−O(2A)	89.9(2)
O(1)−Ru(1)−O(2A)	175.5(2)	O(4)−Ru(1)−O(5A)	175.5(2)
O(1)−Ru(1)−O(5A)	90.0(2)	O(2A)−Ru(1)−O(5A)	89.2(2)
O(4)−Ru(1)−O(10B)	90.1(2)	O(1)−Ru(1)−O(10B)	88.7(2)
O(2A)−Ru(1)−O(10B)	86.9(2)	O(5A)−Ru(1)−O(10B)	85.4(2)
O(4)−Ru(1)−Ru(1)	92.1(2)	O(1)−Ru(1)−Ru(1A)	91.4(2)
O(2A)−Ru(1)−Ru(1A)	93.0 (2)	O(5A)−Ru(1)−Ru(1A)	92.4(2)
O(10B)−Ru(1)−Ru(1A)	177.8(1)	O(12C)−Ru(2)−O(9C)	89.2(2)
O(12C)−Ru(2)−O(8)	90.0(2)	O(9C)−Ru(2)−O(8)	175.8(2)
O(12C)−Ru(2)−O(11)	175.3(2)	O(9C)−Ru(2)−O(11)	89.5(2)
O(8)−Ru(2)−O(11)	91.1(2)	O(12C)−Ru(2)−O(3)	90.6(2)
O(9C)−Ru(2)−O(3)	89.6(2)	O(8)−Ru(2)−O(3)	86.3(2)
O(11)−Ru(2)−O(3)	84.9(2)	O(12C)−Ru(2)−Ru(2C)	92.3(2)
O(9C)−Ru(2)−Ru(2C)	91.8(2)	O(8)−Ru(2)−Ru(2C)	92.4(2)
O(11)−Ru(2)−Ru(2C)	92.2(2)	O(3)−Ru(2)−Ru(2C)	176.8(1)
P(1)−O(1)−Ru(1)	115.8(3)	P(1)−O(2)−Ru(1A)	113.8(3)
P(1)−O(3)−Ru(2)	133.4(3)	P(2)−O(4)−Ru(1)	114.2(3)
P(2)−O(5)−Ru(1A)	113.7(3)	P(3)−O(8)−Ru(2)	113.9(3)
P(3)−O(9)−Ru(2C)	114.7(3)	P(3)−O(10)−Ru(1D)	136.0(3)
P(4)−O(11)−Ru(2)	112.0(3)	P(4)−O(12)−Ru(2C)	113.4(3)

[a] Symmetry codes: (A) $-x, -y+2, -z$; (B) $x, y+1, z$; (C) $-x+1, -y+1, -z$; (D) $x, y-1, z$.

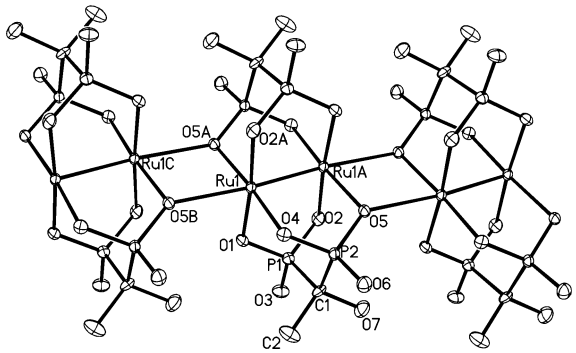

Figure 1. A fragment of the $\{Ru_2(hedp)_2\}_n^{4n-}$ chain in **1** with atom labeling scheme (50% probability).

Each $hedp^{4-}$ in **1** again behaves as a bis(chelating) bridging ligand by using four of its phosphonate oxygens [O(1), O(2), O(4), O(5)] and links two Ru atoms in a cis-bridging mode into a $Ru_2(hedp)_2^{4-}$ dimer. An inversion center sits in the middle of the Ru−Ru edge. The P−O(Ru) distances [1.539-

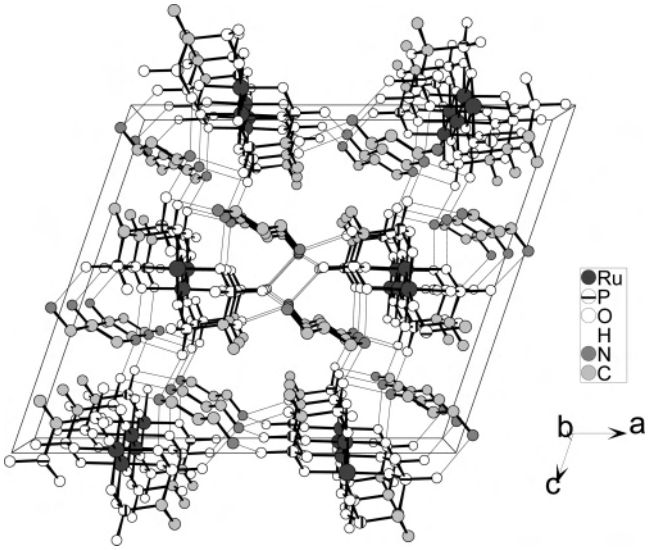

Figure 2. Packing diagram of **1** projected down the *b*-axis.

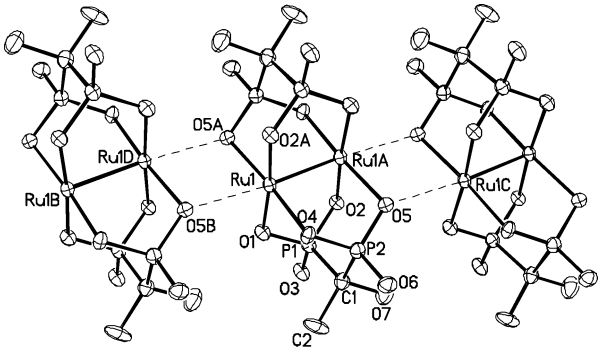

Figure 3. A fragment of the $\{Ru_2(hedp)_2\}_n^{4n-}$ chain in **2** with atom labeling scheme (50% probability).

(4)−1.546(4) Å] are longer than those of the terminal P═O [1.497(4), 1.516(4) Å]. In fact, the phosphonate oxygen O(5) serves as a μ_3-O and further coordinates to the Ru atoms from the neighboring $Ru_2(hedp)_2^{4-}$ unit, leading to the formation of a linear chain along the *b*-axis. This chain is reminiscent of those in compounds $[NH_3(CH_2)_2NH_3][Cu_2(hedp)_2]\cdot H_2O$ and $[NH_3CH(CH_3)NH_3]_2[Cu_2(hedp)_2]$,[26] although no metal−metal bonds are found in the latter cases. The Ru···Ru distance over the μ_3−O(5) bridge is 3.421 Å. In the crystal lattice, these polymeric $\{Ru_2(hedp)_2\}_n^{4n-}$ chains are separated by the protonated 1,3-diaminopropane. Extensive hydrogen bonds are present among the phosphonate oxygens, the hydroxy oxygen, and the ammonium nitrogen atoms (Figure 2).

Description of Structures 2 and 3. Compounds **2** and **3** are isostructural, crystallizing in monoclinic space group $P2_1/n$. Both contain a homovalent dimer unit of $Ru_2(hedp)_2^{4-}$, analogous to compound **1** (Figure 3). The Ru−Ru bond lengths within the paddlewheel cores are 2.338(1) Å for **2** and 2.330(1) Å for **3**. Neighboring dimers are again connected through edge-sharing of ruthenium octahedra, forming chains along the *a*-axis. The Ru(1)−O(5B) bond distances in **2** [2.514(3) Å] and **3** [2.446(5) Å] are longer than that in **1** [2.373(4) Å]. In fact, the Ru(1)−O(5B) distance in **2** may be too long to be considered as a bond. The Ru1···Ru1D distances over the oxygen bridge are 3.588 Å for **2** and 3.491 Å for **3**, respectively. The protonated 1,4-diaminobutane or 1,5-diaminopentane as well as the lattice water molecules fills in the interchain spaces with extensive hydrogen-bond interactions. Figure 4 shows the packing diagram of compound **2**.

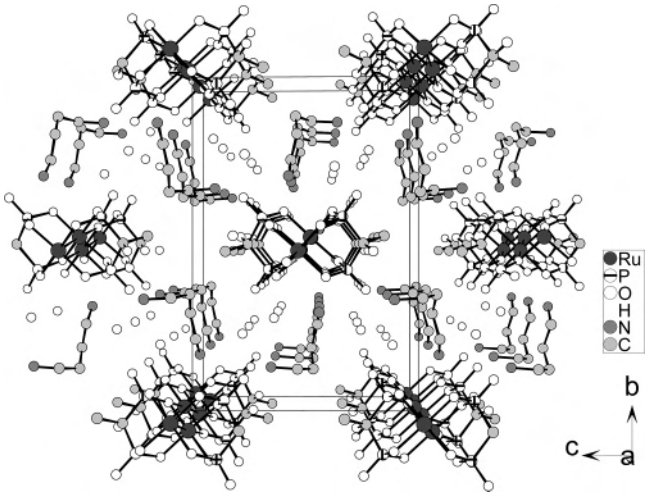

Figure 4. Packing diagram of **2** projected down the *a*-axis.

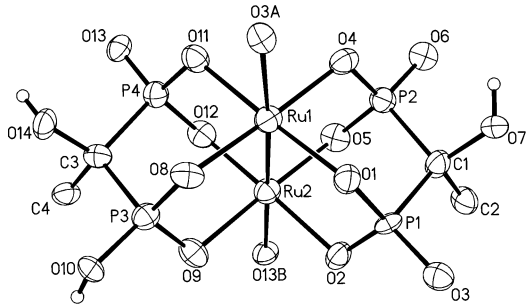

Figure 5. The dimer unit of $Ru_2(hedp)(hedpH)^{2-}$ in **4** with atomic labeling scheme (50% probability).

Description of Structure 4. Compound **4** crystallizes in orthorhombic space group $Pca2_1$. The asymmetric unit contains a $[NH_3(CH_2)_3NH_3]^{2+}$ cation, a mixed-valent diruthenium unit of $Ru_2^{II,III}(hedp)(hedpH)^{2-}$ and a lattice water molecule. Within the $Ru_2(hedp)(hedpH)^{2-}$ unit, there are two crystallographically different Ru atoms (Figure 5). Each has a distorted octahedral geometry. The equatorial positions of $\{Ru(1)O_5Ru\}$ and $\{Ru(2)O_5Ru\}$ octahedra are occupied by the phosphonate oxygen atoms O(1), O(4), O(8), and O(11) and O(2), O(5), O(9), and O(12), respectively. The axial positions are filled with O(3A) and O(13B) from neighboring $Ru_2(hedp)(hedpH)^{2-}$ units. The Ru(1)−O and Ru(2)−O bond lengths are 2.019(6)−2.245(6) and 2.040(5)−2.245(6) Å, respectively, which are too close to clearly identify the oxidation state of each Ru atom. The Ru(1)−Ru(2) distance is 2.360(1) Å, longer than that in homovalent compound **1** [Ru(1)−Ru(1A) distance is 2.330(1) Å], and the mixed-valent compound $(NH_4)_3Ru_2(hedp)_2\cdot 2H_2O$ [Ru(1)−Ru(1A) distance is 2.347(1) Å].[22a] Both $hedp^{4-}$ and $hedpH^{3-}$ ligands serve as bis(chelating) bridging ligands by using four of their six

(26) Song, H.-H.; Zheng, L.-M.; Liu, Y.-J.; Xin, X.-Q.; Jacobson, A. J.; Decurtins, S. *J. Chem. Soc., Dalton Trans.* **2001**, 3274.

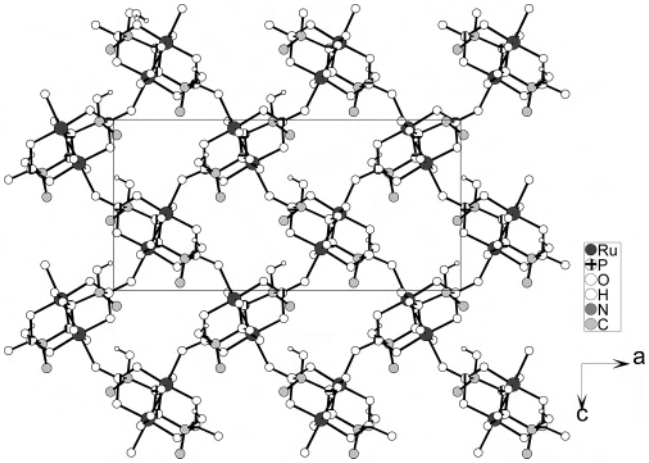

Figure 6. One layer of $\{Ru_2(hedp)(hedpH)\}_n^{2n-}$ in **4** viewed down the *b*-axis.

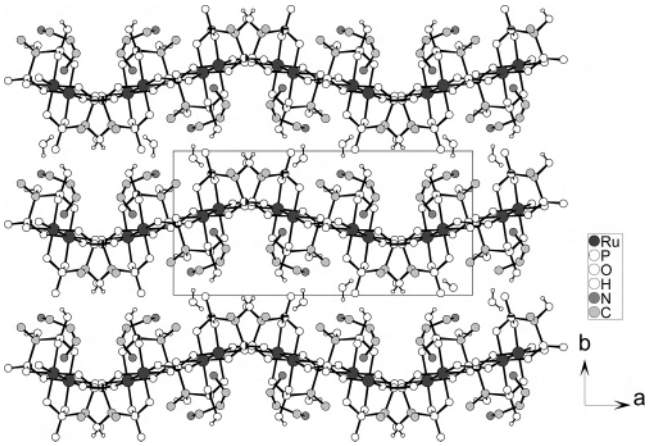

Figure 7. Packing diagram of **4** projected down the *c*-axis showing the undulating arrangement of the layers, and the 1,3-diammoniumpropane cations hydrogen-bonded to the same diruthenium diphosphonate layer and lattice water molecules.

phosphonate oxygen atoms [O(1), O(2), O(4), and O(5) and O(8), O(9), O(11), and O(12), respectively], and link the Ru(1) and Ru(2) atoms into a paddlewheel dimer unit. The adjacent dimer units are connected through phosphonate oxygen atoms O(3) and O(13), forming a distorted square-grid layer in the *ac* plane with composition $\{Ru_2(hedp)(hedpH)\}_n^{2n-}$ (Figure 6). The remaining two phosphonate oxygen atoms within the unit are either protonated [P(3)−O(10), 1.544(5) Å] or pendant [P(2)−O(6), 1.491(5) Å]. The $\{Ru_2(hedp)(hedpH)\}_n^{2n-}$ layer is not planar. Instead, it undulates along the *a*-axis. Each protonated 1,3-diaminopropane is locked within the same layer by hydrogen-bonding with the phosphonate oxygen atoms (Figure 7). The N···O distances are 2.897(9) Å for N(1)···O(9^{i}), 2.800(9) Å for N(1)···O($1w^{ii}$), 2.776(9) Å for N(1)···O(6^{iii}), 3.025(9) Å for N(2)···O(13^{iv}), 2.824(9) Å for N(2)···O(3), and 2.974(9) Å for N(2)···O(12^{iv}) (symmetry codes: (i) $-x + {}^3/_2$, y, $z - {}^1/_2$; (ii) $x + 1$, y, z; (iii) $-x + {}^3/_2$, $y + 1$, $z - {}^1/_2$; (iv) $x + {}^1/_2$, $-y + 1$, z).

Description of Structure 5. Compound **5** crystallizes in trigonal space group $P\bar{3}1c$. In this case, the paddlewheel units of $Ru_2^{II,III}(hedpH_{0.5})_2^{2-}$ are connected by the phosphonate oxygen atoms forming a typical kagomé lattice containing

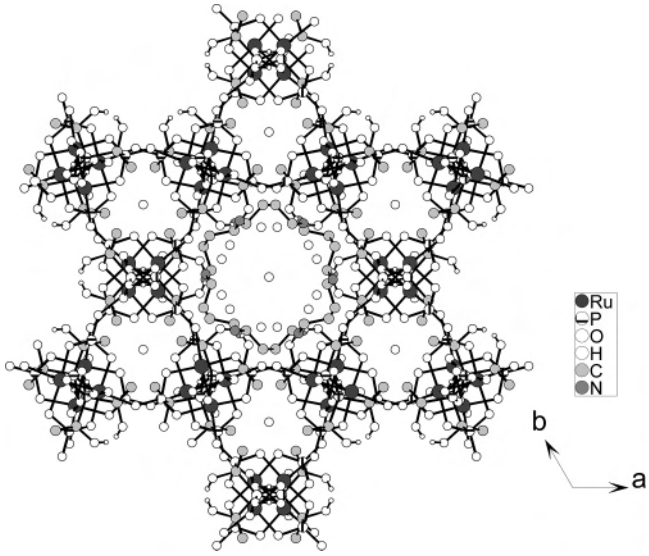

Figure 8. View down the *c*-axis showing the kagomé lattice in **5**, and the 1,4-diammoniumbutane located on the sidewalls of the hexagonal channels and lattice water molecules.

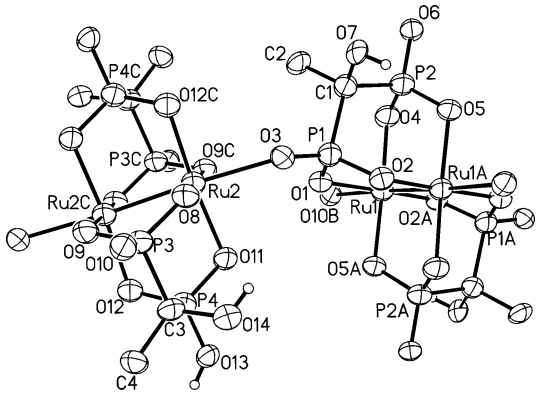

Figure 9. The building unit of $\{[Ru_2(hedp)_2][Ru_2(hedpH)_2]\}^{4-}$ in **6** with atomic labeling scheme (50% probability).

trigonal and hexagonal rings with a composition of $\{Ru_2(hedpH_{0.5})_2\}_n^{2n-}$. Details of the structure have been described in the Communication.[22c] In this structure, the Ru−O bond lengths are in the range 2.018(3)−2.237(3) Å and the Ru(1)−Ru(1A) distance is 2.351(1) Å. The layers are linked by very strong hydrogen bonds, leading to a three-dimensional nanoscale kagomé structure with trigonal and hexagonal channels generated along the *c*-axis. Figure 8 shows clearly that the protonated 1,4-diaminobutane is locked on the sidewalls of the hexagonal channels through hydrogen bonds.

Description of Structure 6. Compound **6** crystallizes in triclinic space group $P\bar{1}$. The asymmetric unit contains a $[NH_3(CH_2)_5NH_3]^{2+}$ cation, two Ru atoms, one $hedp^{4-}$, and one $hedpH^{3-}$ group. In this compound, two equivalent $hedp^{4-}$ (or $hedpH^{3-}$) groups bis(chelate) and bridge the equivalent Ru(1) [or Ru(2)] atoms, forming $Ru(1)_2(hedp)_2^{3-}$ [or $Ru(2)_2(hedpH)_2^{-}$] paddlewheel cores (Figure 9). These cores are interconnected by phosphonate oxygen atoms O(3) and O(10), forming a distorted square-grid layer similar to that observed in compound **4** (Figure 10). The Ru−O bond lengths are in the range of 2.025(5)−2.299(5) Å, consistent

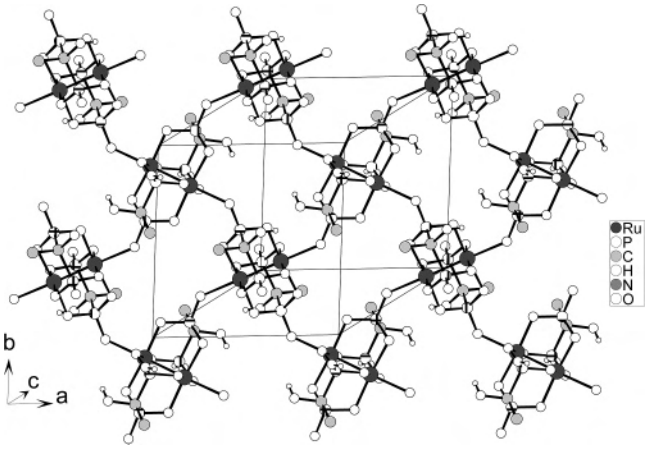

Figure 10. One layer of $\{[Ru_2(hedp)_2][Ru_2(hedpH)_2]\}_n^{4n-}$ in **6**.

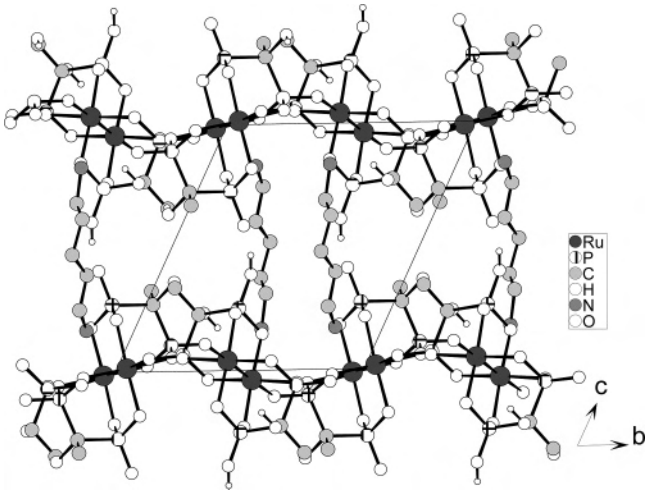

Figure 11. Packing diagram of **6** projected down the *a*-axis showing the 1,5-diammoniumpentane "pillars" located between the layers.

with those in **4**. The Ru(1)−Ru(1A) and Ru(2)−Ru(2C) distances are 2.346(1) and 2.366(1) Å, respectively. A significant feature of compound **6** is that the protonated 1,5-diaminopentane behaves like a pillar. Its two terminal nitrogen atoms are hydrogen-bonded to the phosphonate oxygen atoms from the neighboring layers, forming a three-dimensional "pillared" layered structure (Figure 11). The shortest N···O contacts are 2.888(7) Å for N(1)···O(2^{i}), 2.932(8) Å for N(1)···O(3^{ii}), 2.860(7) Å for N(2)···O(9^{iii}), and 2.895(7) Å for N(2)···O(10^{iv}) (symmetry codes: (i) $-x$, $-y+1$, $-z+1$; (ii) x, y, $z+1$; (iii) $-x+1$, $-y+1$, $-z$; (iv) x, $y+1$, z).

Template and pH Influences. Usually the template effect depends on both its own properties and the nature of the anionic lattice.[27] The former includes the size, geometrical shape, hydrogen-bonding ability with the other components, and charge density and distribution. For the flexible organic diamines $NH_2(CH_2)_nNH_2$ ($n = 3-5$) used as templates in this work, all can be diprotonated under acidic conditions and form extensive hydrogen bonds with the phosphonate or hydroxy oxygen atoms. The size and the geometrical shape should be essential in directing the structures of the corresponding Ru_2-hedp compounds. Compounds **4** and **6**, containing similar distorted square-grid anionic layers, provide good examples showing template effect. In **4**, the protonated 1,3-diaminopropane with a smaller size is arranged in a cis manner and is hydrogen-bonded to the phosphonate oxygen atoms from the same anionic layer by using its two terminal nitrogen atoms, hence forming a strongly undulating layer in the *ac* plane. In **6**, the protonated 1,5-diaminopentane with a larger size is arranged in a trans manner and is hydrogen-bonded to the phosphonate oxygen atoms from the two neighboring anionic layers, thus forming a "pillared" layered structure. Compound **5** exhibits a unique kagomé lattice, remarkably different from those of **4** and **6**. The suitable size and the flexibility of the protonated 1,4-diaminobutane, which is locked on the sidewalls of the hexagonal channels within the layer, should be a key in forming this structure.

(27) Zheng, L.-M.; Song, H.-H.; Xin, X.-Q. *Comments Inorg. Chem.* **2000**, *22*−*24*, 129.

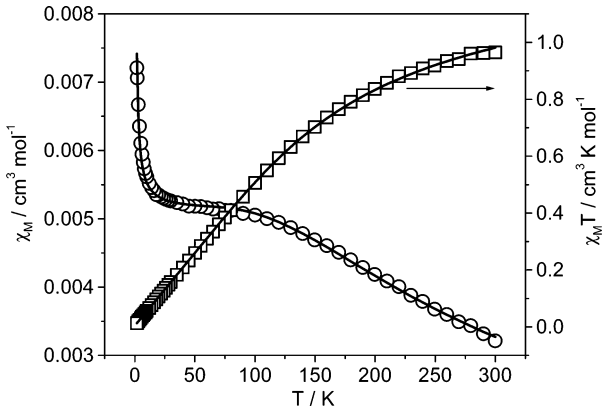

Figure 12. The χ_M and $\chi_M T$ vs T plots for **2**.

The effect of pH is also significant. At a lower pH (ca. 2.5 to ~4 for **4** and **5**, 4 to ~5 for **6**), mixed-valent compounds **4**−**6** with layer structures were produced, whereas at a higher pH (ca. 6), homovalent compounds **1**−**3** with chain structures were obtained. The result indicates that the low oxidation state of the diruthenium(II,II) unit can be stabilized, and the formation of chain structures can be promoted at a higher pH when the organic diamines are present. The mechanism, however, is still not clear to us.

Magnetic Properties. The temperature-dependent magnetic susceptibilities of compounds **1**−**6** were investigated in the temperature range 1.8 to 300 K at 2 kOe. For the homovalent diruthenium(II,II) diphosphonate compounds **1**−**3**, the observed effective magnetic moments per Ru_2 at 300 K are 3.01 μ_B for **1**, 2.78 μ_B for **2**, and 2.78 μ_B for **3**, respectively, corresponding to two unpaired electrons expected for a homovalent $Ru_2^{II,II}$ unit (2.828 μ_B for $S = 1$). For the mixed-valent diruthenium(II,III) diphosphonate compounds **4**−**6**, the observed effective magnetic moments per Ru_2 at 300 K are 4.13 μ_B for **4**, 4.31 μ_B for **5**, and 4.27 μ_B for **6**, respectively, corresponding to three unpaired electrons expected for a mixed-valent $Ru_2^{II,III}$ unit (3.87 μ_B for $S = {}^3/_2$).

Figure 12 shows the χ_M and $\chi_M T$ versus T curves for compound **2**. As the compound is cooled, the $\chi_M T$ value decreases continuously from 0.96 cm^3 K mol^{-1} at 300 K to

0.013 cm^3 K mol^{-1} at 1.8 K, primarily due to the ZFS arising from the $^3A_{2g}$ ground state. The susceptibility data were fitted by the following equation:[19a]

$$\chi''_{Ru_2} = (1 - \rho)\chi'_{Ru_2} + \rho(5Ng_{imp}{}^2\beta^2/(4k_BT))$$

where ρ is the paramagnetic impurity, and χ' includes the antiferromagnetic coupling (zJ). Thus

$$\chi'_{Ru_2} = \chi_{Ru_2}/[1 - (2zJ/(Ng^2\beta^2))\chi_{Ru_2}]$$

where

$$\chi_{Ru_2} = \frac{2Ng^2\beta^2}{3k_BT}\frac{\exp(-D/(k_BT)) + ((2k_BT)/D)(1 - \exp(-D/(k_BT))}{1 + 2\exp(-D/(k_BT))} + \text{TIP}$$

The best fit, shown as the solid line in Figure 12, results in parameters $g = 2$ (fixed), $D = 280$ cm^{-1}, $zJ = -3.91$ cm^{-1}, TIP $= 3.6 \times 10^{-4}$ cm^3 mol^{-1}, and $\rho = 0.17\%$. For compounds **1** and **3**, the parameters are $g = 2$ (fixed), $D = 249$ cm^{-1}, $zJ = -2.35$ cm^{-1}, TIP $= 3.7 \times 10^{-4}$ cm^3 mol^{-1}, and $\rho = 9.2\%$ and $g = 2$ (fixed), $D = 302$ cm^{-1}, $zJ = -3.52$ cm^{-1}, TIP $= 3.7 \times 10^{-4}$ cm^3 mol^{-1}, and $\rho = 0.12\%$, respectively (Figures S2 and S3, Supporting Information).

Figure 13 shows the $\chi_M T$ versus T curves for compound **4**. As the compound is cooled, the $\chi_M T$ value decreases smoothly from 2.16 cm^3 K mol^{-1} at 300 K to a minimum of 1.45 cm^3 K mol^{-1} at 12 K below which $\chi_M T$ increases rapidly and reaches 1.84 cm^3 K mol^{-1} at 1.8 K. The continuous decreasing of $\chi_M T$ is due to the large zero-field splitting (D) arising from the $S = {}^3/_2$ ground state of Ru_2^{5+}. The upturn below 12 K could be caused by the interdimer ferromagnetic interactions. Similar behaviors are also observed for compounds **5** [22c] and **6** (Figure S4). The magnetic susceptibility data of compounds **4**−**6** can be analyzed by the following equations:[12a]

$$\chi_{Ru_2} = \frac{Ng^2\beta^2}{k_BT}\left[\frac{1}{3}\frac{1 + 9\exp(-2D/(k_BT))}{4(1 + \exp(-2D/(k_BT)))} + \frac{2}{3}\frac{1 + (3k_BT/(4D))(1 - \exp(-2D/(k_BT)))}{1 + \exp(-2D/(k_BT))}\right] + \text{TIP}$$

$$\chi'_{Ru_2} = \chi_{Ru_2}/[1 - (2zJ/(Ng^2\beta^2))\chi_{Ru_2}]$$

where N, g, β, and k_B have their usual meanings, and zJ accounts for the magnetic interactions between the paramagnetic centers. TIP represents the temperature independent paramagnetism of the compound. The best fit for compound **4** is shown as the solid line in Figure 13, with parameters $g = 2.15$, $D = 94.8$ cm^{-1}, $zJ = 0.26$ cm^{-1} and TIP $= 2.7 \times 10^{-5}$ cm^3 mol^{-1}. For compounds **5** and **6**, the parameters are $g = 2.25$, $D = 95.1$ cm^{-1}, $zJ = 0.25$ cm^{-1}, and TIP $= 3.3 \times 10^{-5}$ cm^3 mol^{-1} and $g = 2.24$, $D = 96.5$ cm^{-1}, $zJ =$ 0.27 cm^{-1}, and TIP $= 5.6 \times 10^{-6}$ cm^3 mol^{-1}, respectively. The positive θ values are in accordance with the presence of weak ferromagnetic interdimer interactions in **4**−**6**. Both the D and θ values of **4**−**6** are comparable to those for $(NH_4)_3Ru_2(hedp)_2 \cdot 2H_2O$.[22a]

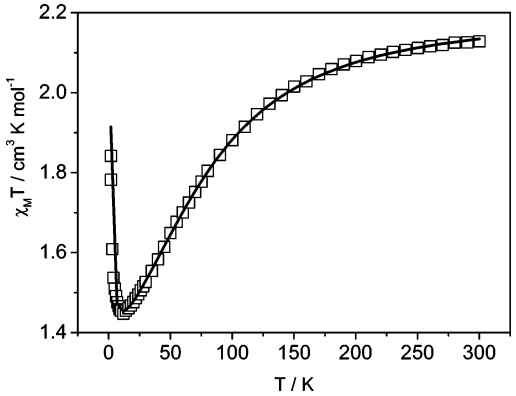

Figure 13. The $\chi_M T$ vs T plot for **4**.

Conclusion. Three homovalent diruthenium(II,II) diphosphonates $[H_3N(CH_2)_3NH_3]_2[Ru_2(hedp)_2]$ (**1**), $[H_3N(CH_2)_4NH_3]_2[Ru_2(hedp)_2]\cdot 4H_2O$ (**2**), and $[H_3N(CH_2)_5NH_3]_2[Ru_2(hedp)_2]\cdot 4H_2O$ (**3**) and three mixed-valent diruthenium(II,III) diphosphonates, namely, $[H_3N(CH_2)_3NH_3][Ru_2(hedp)(hedpH)]\cdot H_2O$ (**4**), $[H_3N(CH_2)_4NH_3][Ru_2(hedpH_{0.5})_2]\cdot 2H_2O$ (**5**), and $[H_3N(CH_2)_5NH_3]_2\{[Ru_2(hedp)_2][Ru_2(hedpH)_2]\}$ (**6**) (hedp = 1-hydroxyethylidenediphosphonate) have been synthesized and structurally characterized. Compounds **1**−**3** exhibit analogous linear chain structures with the protonated organic diammonium cations locate between the chains. Layer structures are found in the mixed-valent compounds **4**−**6**. Compounds **4** and **6** have square-grid layer structures with the protonated 1,3-diaminopropane and 1,5-diaminopentane hydrogen-bonded to the single layer and neighboring two layers, respectively. Compound **5** shows a kagomé layer structure with the protonated 1,4-diaminobutane residing on the sidewall of the hexagonal channels through hydrogen-bond interactions. The presence of organic templates and the pH of the reaction mixtures are responsible for the formation of these compounds with different topologies and oxidation states. The variable-temperature magnetic susceptibility measurements show that antiferromagnetic exchanges are mediated between the $Ru_2^{II,II}$ dimers in compounds **1**−**3**, while ferromagnetic interactions exist between the $Ru_2^{II,III}$ dimers in compounds **4**−**6**.

Acknowledgment. This work was funded by the NNSF of China (Grant No. 20325103) and the Ministry of Education of China. The authors thank Mr. Yong-Jiang Liu for crystal data collections.

Supporting Information Available: Crystallographic files in CIF format and three figures. This material is available free of charge via the Internet at http://pubs.acs.org.

IC060041H